# Electronic Supplementary Information (ESI)

## Solar-Driven Tripus Photocatalytic Action of Defective S-doped g-$C_3N_4$ for 1,4 NADH Regeneration and Simultaneous Benzylamine Conversion with $CO_2$ Fixation into HCOOH

Kanchan Sharma [a], Rajesh K. Yadav*[a] , Rajesh K. Verma *[b], Satyam Singh[d] , Shaifali Mishra[a] , Rehana Shahin[a] , Atul P. Singh[e] , Chandani Singh[c] , Navneet K. Gupta[d] , Jin-OoK Baeg *[c] , Hwanhui Yun[c], Hyeongjoong Kim[c]

[a]*Department of Chemistry and Environmental Science, Madan Mohan Malaviya University of Technology, Gorakhpur, 273010, (U.P.), India. *Email: rajeshkr_yadav2003@yahoo.co.in.

[b]*Department of Mechanical Engineering, School of Engineering, Harcourt Butler Technical University, Kanpur, India- 208002

[c]*Korea Research Institute of Chemical Technology, N3, 141 Gajeong-ro, Yuseong-gu, Daejeon 34114, KoreaSouth Korea. *Email: jobaeg@krict.re.kr;

Email: yhh1217@krict.re.kr, Email: kimhj@krict.re.kr

[d]Centre for Sustainable Technologies, IISC Bangalore Gulmohar Marg, Bengaluru 560012, India

[e]Department of Chemistry, Central University of South Bihar, Gaya, 823001, India

## Content

## 1. General remarks

Melamine, thiourea, sodium borohydride ($NaBH_4$), Nicotinamide adenine dinucleotide ($NAD^+$), carbon-dioxide gas, benzylamine, 2-methyl benzylamine, 4-chlorobenzylamine, 4 fluorobenzyl amine, 4-methoxybenzylamine, acetonitrile, ethanol, tetrahydrofuran (THF), dimethyl sulfoxide (DMSO), dimethylformamide (DMF), methanol, Rh compound ($[Rh(C_5Me_5)\ Cl_2]_2$), 2,2'-bipyridyl, ascorbic acid all purchased from Sigma Aldrich and used in the reaction without further purification. The Rh complex and buffer solution was synthesized in the laboratory.

# 2. Instruments and measurements

Shimadzu UV-1800 spectrometer was used to record UV-DRS (UV- diffraction reflectance spectroscopy) and UV- Visible spectroscopy. Fourier transform infrared (FTIR) spectroscopy was performed using a Thermo Scientific Nicolet 6700 spectrometer with KBr pellet support. Powder X-ray diffraction (XRD) analysis utilized a Bruker AXS D8 Advance X-ray diffractometer equipped with Cu Kα radiation. Scanning electron microscope (SEM) images were captured on a Phillips FET instrument (Model No. 200kV LAB6, FEL TECNAI G2-20S-Twin) operating at 200 kV. Tafel plots, and Electrochemical Impedance Spectroscopy (EIS) were performed using a CHI608E instrument. Proton nuclear magnetic resonance (1H NMR) spectra were recorded on a Bruker AVANCE II + 300 MHz spectrometer with tetramethylsilane (TMS; $\delta = 0$) as the internal standard. X-ray photoelectron spectroscopy (XPS) was performed using an Escalab 250Xi instrument from Thermo Fisher. Brunauer–Emmett–Teller (BET) analysis was performed using the Quantachrome Autosorb iQ3 instrument and Electron paramagnetic resonance (EPR) was performed using Bruker Win EPR. Photoluminescence spectrum measurements were taken by Perkin Elmer LS-55. Photocurrent measurements were performed using an electrochemical analyzer (CHI Instrument 1100A).

## 3. Recyclability and Physiochemical stability of Defective S-doped g-$C_3N_4$ (DSGN) photocatalyst

The recyclability of the DSGN photocatalyst for % NADH regeneration was evaluated by filtering and collecting the DSGN photocatalyst after each catalytic process, followed by thorough washing with excess water. After drying it in an oven, the photocatalyst was reused for subsequent cycles of NADH regeneration. The reaction cycle was repeated for five consecutive cycles in a row to assess the photocatalytic activity of the recovered catalyst. The photo-catalytic efficiency of DSGN photocatalyst remains consistent for up to five consecutive experiments, as shown in Figure S1(a). The physio-stability DSGN photocatalyst for simultaneous $CO_2$ and benzylamine conversion was evaluated by filtering and collecting the used DSGN photocatalyst. After thorough washing of DSGN photocatalyst with excess amount of organic solvent and drying it in oven, its FTIR spectra was recorded. The FTIR spectra of the DSGN photocatalyst was analyzed before and after its application in the simultaneous conversion of benzylamine to imine and the fixation of $CO_2$ to HCOOH as shown in figure S1(b). The comparison of these spectra reveals that are no significant changes in the characteristic absorption bands, suggesting that the chemical structure of the DSGN photocatalyst remain intact after the photocatalytic process. The stability is important for its potential reuse in the photocatalytic applications ensuring consistent performance over numerous cycles without degradation or loss of activity. [1–4]

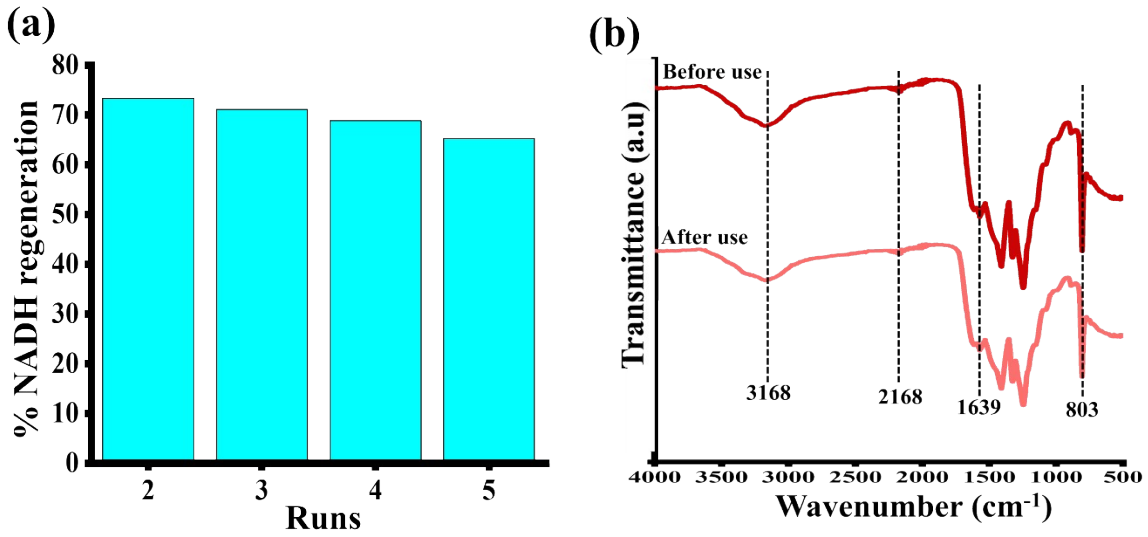


**Figure S1**. (a) Recyclability for NADH regeneration of DSGN photocatalyst. (b) Physiochemical stability through FTIR of DSGN photocatalyst for simultaneous $CO_2$ fixation to HCOOH along with benzylamine to imine conversion.

## 4. Determination of yield of formic acid (HCOOH) using UV-vis spectroscopy

A calibration plot illustrated in figure S3 (a) was used to calculate the yield of HCOOH produced in the reaction. This curve was plotted between the known concentration of HCOOH and the optical density (O.D) or absorbance values obtained from UV-vis spectra, which aided in the determination of the produced HCOOH concentrations.[5–8] Figure S3 (b) demonstrate the UV-vis spectra of pure benzylamine, pure formic acid and reacting mixture after the completion of the reaction in acetonitrile under $CO_2$ gas with DSGN photocatalyst.

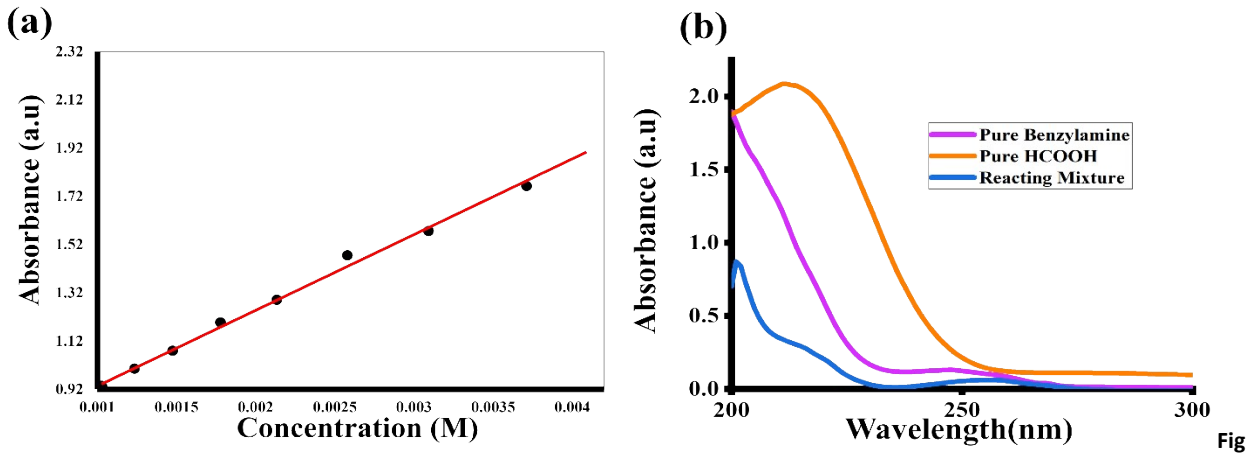


**Figure S2. (a)** Calibration curve of HCOOH acid for the determination of HCOOH produced in the reaction **(b)** UV-vis spectra of pure benzylamine, pure HCOOH and reacting mixture after completion of the reaction in acetonitrile under $CO_2$ gas with DSGN photocatalyst.

## 5. Synthesis of Bulk g-$C_3N_4$ and its photocatalytic NADH regeneration performance

The bulk g-$C_3N_4$ was prepared as per reported paper.[9] Specifically, 3g of melamine was directly pyrolyzed in a muffle furnace at 600°C for 4h at a ramping rate of 3°C /min. The light-yellow solid product obtained was bulk g-$C_3N_4$. This bulk g-$C_3N_4$ was tested for photocatalytic NADH regeneration under solar light illumination in a quartz reactor, which contained a mixture of NAD+ (243 µL), a Rh complex mediator (124 µL), ascorbic acid (310 µL), and 10 mg of bulk g-$C_3N_4$ in 3.1 mL of sodium phosphate buffer (100 mM, pH 7.0). The reaction was conducted under an inert atmosphere at room temperature. Initially, the system was allowed to equilibrate in the dark for 30 minutes, during which no NADH formation was detected. Upon exposure to light from a 450 W xenon lamp equipped with a 420 nm cut-off filter, the regeneration of 1,4-NADH was monitored spectrophotometrically. The light-induced regeneration proceeded linearly over time, resulting in a measurable yield of 7.39%. The figure S3 (a) and (b) demonstrate the synthesis of bulk g-$C_3N_4$ and % NADH regeneration yield via bulk bulk g-$C_3N_4$ respectively.

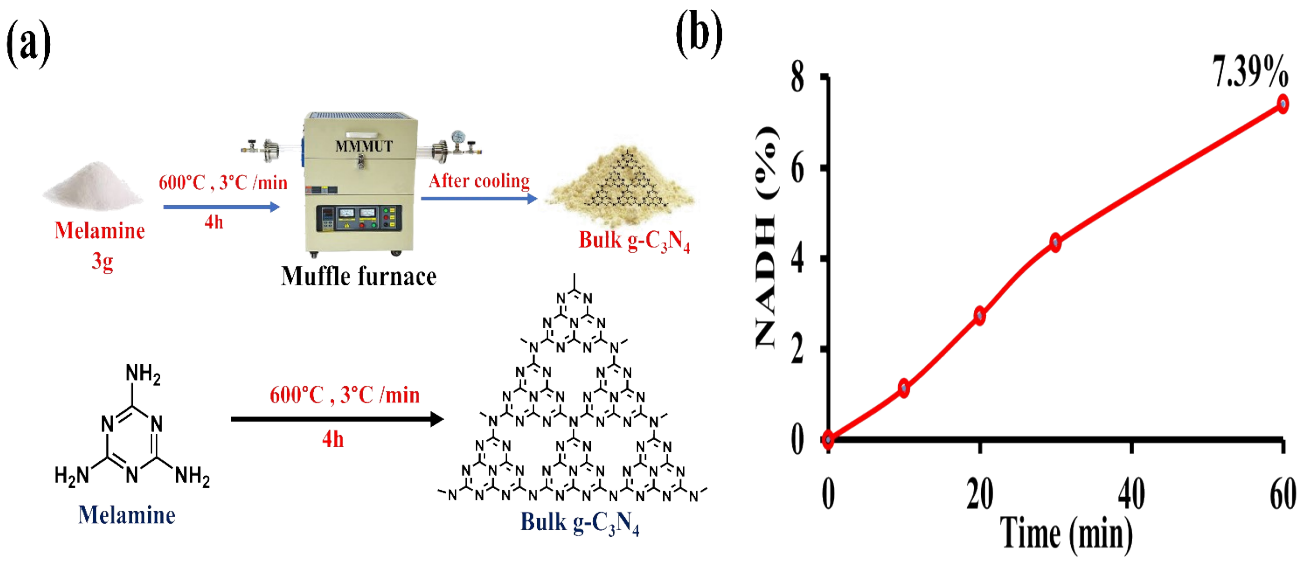


**Figure S3. (a)** Synthesis of bulk g-$C_3N_4$ **(b)** % NADH regeneration via bulk g-$C_3N_4$

## 6. Rh-complex cycle for NADH regeneration by DSGN photocatalyst

The mechanism for photocatalytic NADH regeneration suggests that first, the absorption of photons with energy equal to or greater than the energy band gap of the DSGN photocatalyst triggers the formation of electron-hole pairs in the valence band (VB) of the photocatalyst with a HOMO energy level of -5.52 eV. Ascorbic acid acts as sacrificial agent by donating its electron to quench the VB of DSGN photocatalyst which induces the photo-excited electrons in the VB to jump to the conduction band (CB) of DSGN photocatalyst with a LUMO energy level of -3.38 eV. The photogenerated electron is then transferred to the Rh complex(3.96eV). In the meantime, the cationic form of Rh complex(A) that is present in the reaction mixture forms a water-coordinated complex(B) represented by $[Cp^*Rh(bpy)\ (H_2O)]^{2+}$. This water complex B then reacts with the formate ($HCOO^-$) of ascorbic acid and generates rhodium hydride complex(C) i.e., $[Cp^*Rh(bpy)(H)]^+$ via β-hydrogen

elimination. This process also involves the elimination of $CO_2$. Now the photo-excited electron in the CB of DSGN is taken up by the rhodium hydride complex (C) which gets reduced to complex D. Following this step, the coordination of complex D with $NAD^+$ occurs through the amide functional group, simultaneously facilitating a hydride transfer, that generates NADH.[3,4,10,11]

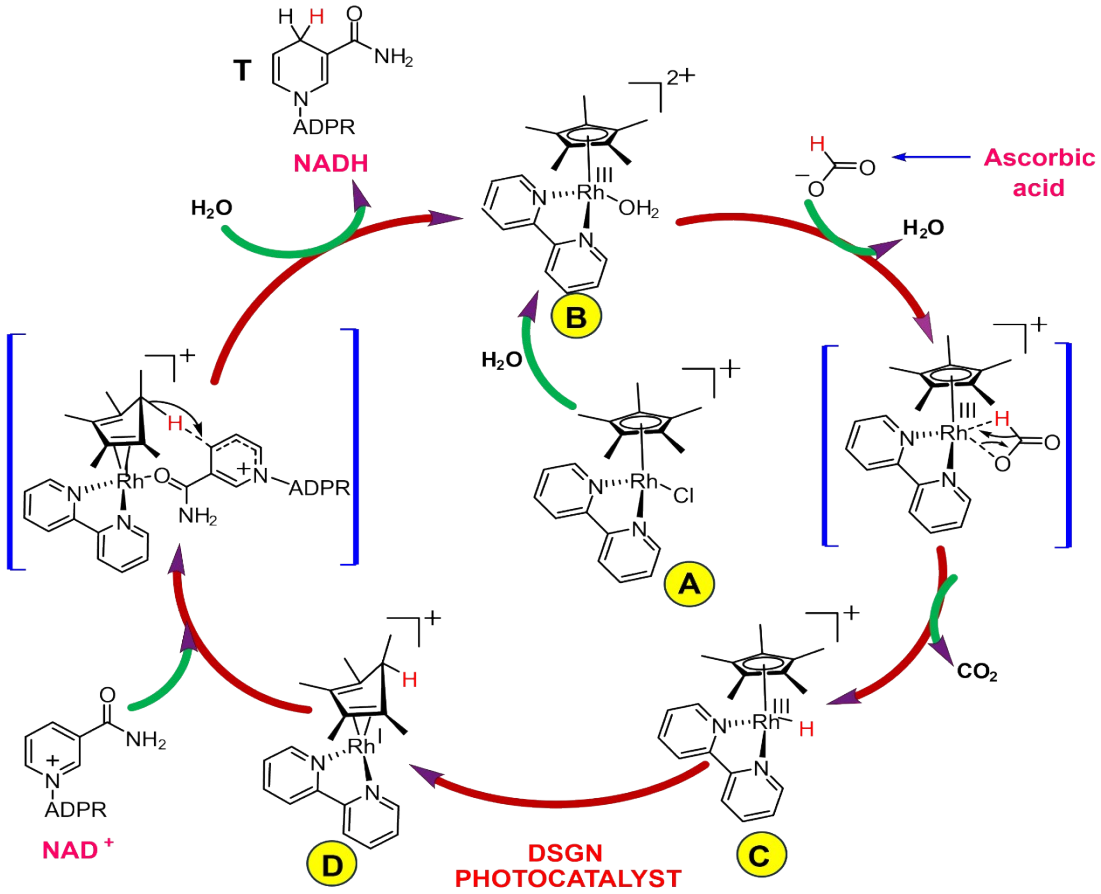


**Figure S4.** Depiction of Rh-complex cycle for NADH regeneration by DSGN photocatalyst.

## 6. Brunauer–Emmett–Teller (BET) analysis of S-doped g-$C_3N_4$ and DSGN photocatalyst

The Brunauer–Emmett–Teller (BET) surface area analysis, as measured by the $N_2$ sorption isotherm, presented in Figure S5 demonstrates that S-doped g-$C_3N_4$ has a surface area of 15.388 $m^2/g$, while DSGN photocatalyst displays a reduced surface area of 4.03 $m^2/g$. This reduction in the surface area for the DSGN photocatalyst may be attributed to aggregation of sample during the treatment sample washing.[12]

| Sample | BET surface area ($m^2/g$) |
|---|---|
| S-doped g-$C_3N_4$ | 15.3881 |
| DSGN photocatalyst | 4.0322 |

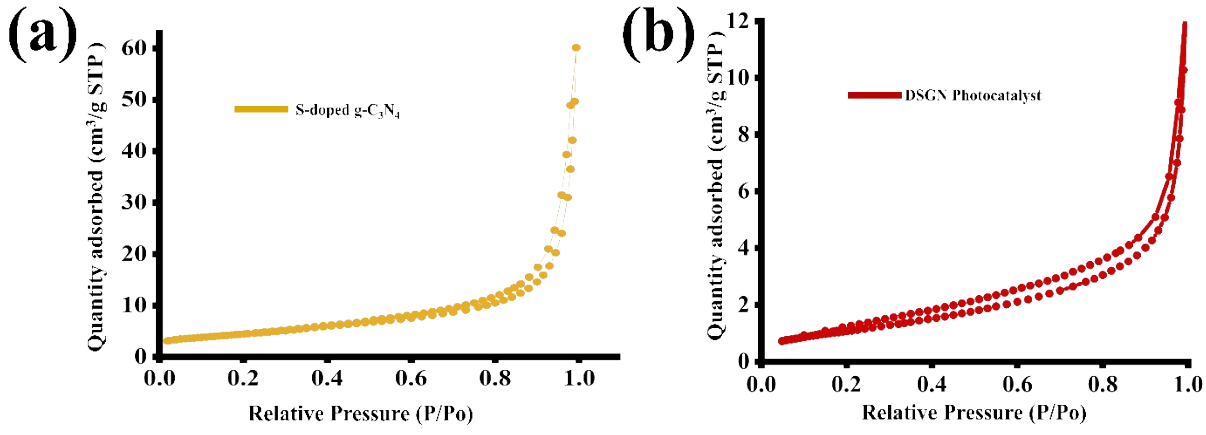


**Figure S5.** BET surface area analysis of (a)S-doped g-$C_3N_4$ and (b)DSGN photocatalyst measured by $N_2$ adsorption-desorption isotherms.

**References**


1 S. Cao, J. Low, J. Yu and M. Jaroniec, 2015, 1–27.

2 R. K. Yadav, J. Baeg, A. Kumar, K. Kong, G. H. Oh and N. Park, 2014, 5068–5076.

3 R. K. Yadav, J. O. Baeg, A. Kumar, K. J. Kong, G. H. Oh and N. J. Park, *J. Mater. Chem. A*, 2014, **2**, 5068–5076.

4 R. K. Yadav, A. Kumar, D. Yadav, N. J. Park, J. Y. Kim and J. O. Baeg, *ChemCatChem*, 2018, **10**, 2024–2029.

5 S. Das, P. Sarkar, A. C. Kothari, M. Goswami, A. Khan and S. M. Islam, *New J. Chem.*, 2024, **48**, 7599–7613.

6 T. A. Yemata, Y. Zheng, A. K. K. Kyaw, X. Wang, J. Song, W. S. Chin and J. Xu, *RSC Adv.*, 2020, **10**, 1786–1792.

7 Y. Nishiwaki-Akine and T. Watanabe, *Green Chem.*, 2014, **16**, 3569–3579.

8 S. Lee, H. Ju, H. Jeon, R. L. Machunda, D. Kim, J. K. Lee and J. Lee, *ECS Trans.*, 2013, **53**, 41–47.

9 N. Rahbar, Z. Salehnezhad, A. Hatamie and A. Babapour, *Microchim Acta* **185**, 101 (2018).

10 S. Singh, R. K. Yadav, T. W. Kim, C. Singh, P. Singh, A. P. Singh, A. K. Singh, A. K. Singh, J. O. Baeg and S. K. Gupta, *React. Chem. Eng.*, 2022, **7**, 1566–1572.

11 J. Agrawal, R. Shahin, C. Singh, S. Singh, R. K. Shukla, S. Mishra, P. Singh, J. O. K. Baeg, R. K. Yadav and N. K. Gupta, *RSC Sustain.*, 2023, 695–700.

12 Y. Wen, D. Qu, L. An, X. Gao, W. Jiang, D. Wu, D. Yang and Z. Sun, *ACS Sustain. Chem. Eng.*, 2019, **7**, 2343–2349.